Annu. Rev. Phys. Chem. 2002. 53:221–47
DOI: 10.1146/annurev.physchem.53.082801.093725


# ELECTRON TRANSFER AT MOLECULE-METAL INTERFACES: A Two-Photon Photoemission Study

X.-Y. Zhu
*Department of Chemistry, University of Minnesota, Minneapolis, Minnesota 55455; e-mail: zhu@chem.umn.edu*



**Key Words** anionic resonance, molecular electronics, interfacial electron transfer, organic semiconductor, unoccupied states

■ **Abstract** Electron transfer between a molecular resonance and a metal surface is a ubiquitous process in many chemical disciplines, ranging from molecular electronics to surface photochemistry. This problem has been probed recently by two-photon photoemission spectroscopy. The first photon excites an electron from an occupied metal state to an unoccupied molecular resonance. Subsequent evolution of the excited electronic wavefunction is probed in energy, momentum, and time domains by the absorption of a second photon, which ionizes the electron for detection. These experiments reveal the important roles of molecule-metal wavefunction mixing, intermolecular band formation, polarization, and localization in interfacial electron transfer.

## INTRODUCTION

What is common to the following interfacial processes? Consider an organic light emitting device or field effect transistor (FET), a molecular switch contacted by two metal electrodes, substrate-mediated surface photochemistry, and solar energy conversion on dye-sensitized semiconductors. All these processes involve electron transfer (ET) between a molecule and a metal or semiconductor surface. In organic light-emitting devices electron injection from a metallic electrode into the lowest unoccupied molecular orbital (LUMO) is a critical step, and the efficiency of the device is intimately related to interfacial ET rate (1, 2). Current understanding of this issue remains at the level of energetics, i.e., the relative position of the LUMO to the metal Fermi level, but the interfacial ET rate is also related to the electronic coupling matrix element as well as the dynamics of electron relaxation and localization. Similar issues are found in organic FETs (3). Interfacial ET is key to the emerging field of molecular electronics. Building a successful molecular electronic device often requires making electronic contacts to one or a group of molecules (4). In this regard electronic coupling between a metal electrode and a molecule determines not only contact resistance but also the nature of the molecular device. In surface photochemistry on metals the transfer of photo-excited substrate electrons

to molecular resonances is believed to be a dominant mechanism, but few experiments have provided direct evidence for such a transient anionic resonance (5). In dye-sensitized solar energy conversion the injection of a photo-excited electron from the LUMO of the dye molecule to the conduction band of the semiconductor, as well as hole injection from the highest occupied molecular orbital to valence band, is the central issue (6, 7). Strong electronic coupling between the two leads to ultrafast ET rates, but the lack of precise control over molecular adsorption in a solution phase experiment makes this a particularly difficult problem. Similar issues are well known in the more mature field of electrochemistry (8).

This account summarizes recent experiments using two-photon photoemission (2PPE) spectroscopy to characterize the electronic structure and ET dynamics at molecule-metal interfaces. Two features of this approach are noteworthy: (*a*) The molecule-surface interaction is well characterized and controlled for a single crystal surface/adsorbate system in an ultrahigh vacuum environment, and (*b*) the 2PPE technique is sensitive to the electronic interaction, i.e., wavefunction overlap, between unoccupied molecular orbitals and substrate band structures and can be applied in a time-resolved manner to directly measure the ultrafast ET rate. The principle of this technique is illustrated in Figure 1.

In Figure 1*a* the molecule interacts strongly with a metal surface, as illustrated by a molecular wavefunction (e.g., LUMO) mixed with the substrate band

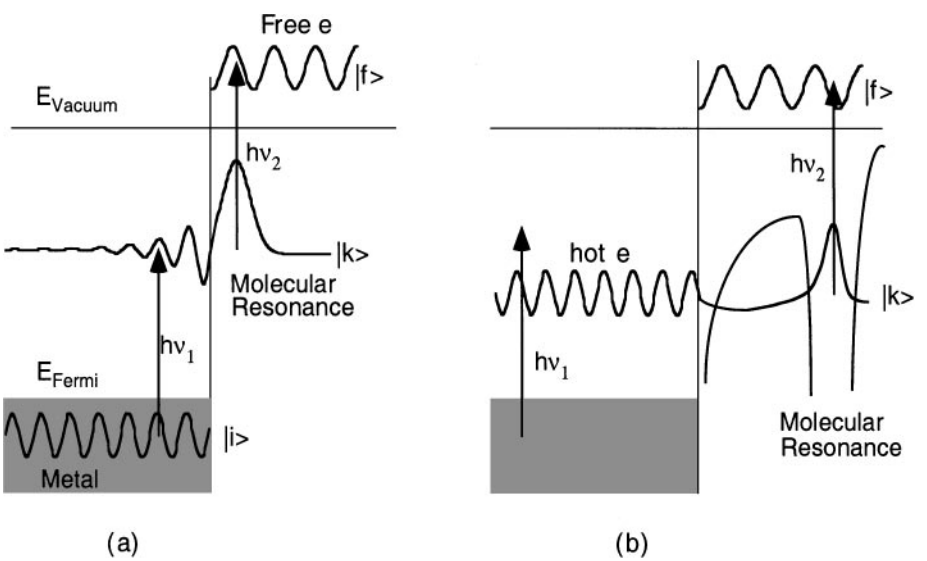


**Figure 1** Schematic illustration of two-photon photoemission via an intermediate molecular resonance, |k⟩, in (*a*) a direct photo-induced electron transfer mechanism and (*b*) an indirect hot-electron transfer mechanism.

structure. Such mixing is represented schematically as an oscillating tail of the wavefunction in the periodic substrate lattice. The first photon excites an electron from an occupied metal state to the mixed molecular state; this is ET from the metal to the molecular resonance. The second photon ionizes the transient molecular anion for detection. The kinetic energy of the photo-emitted electron provides the energetic position of the molecular resonance. For excitation with one-color laser light under the continuous wave (CW) approximation, the rate ($w_{if}$) of such a resonant two-photon ionization process involving an initial metal state $|\mathrm{i}\rangle$, an intermediate molecular resonance $|\mathrm{k}\rangle$, and a final free-electron state $|\mathrm{f}\rangle$ is given in (9) by

$$w_{if} \propto \left|\left(\vec{\mu}_{ik}\cdot\vec{E}\right)\left(\vec{\mu}_{kf}\cdot\vec{E}\right)\right|^2, \qquad 1.$$

where $\mu_{ik}$ and $\mu_{kf}$ are the transition dipole moments for the excitation step and the photo-ionization step, respectively. $\boldsymbol{E}$ is the electric field vector of the laser light. For the molecular resonance to be observable in 2PPE, both $\mu_{ik}$ and $\mu_{kf}$ must be nonzero. This leads to a few requirements on the molecular wavefuction, $|\mathrm{k}\rangle$: (*a*) The molecular wavefunction must possess the right symmetry with respect to the initial metal wavefunction; (*b*) because $|\mathrm{i}\rangle$ is delocalized parallel to the surface plane, the molecular wavefunction must possess nonvanishing dispersion in the surface plane; and (*c*) because the final state is a free-electron wave with certain periodicity (depending on kinetic energy), the spatial modulation or confinement of the molecular wavefunction in the surface normal direction must match that of the free-electron wave to give a nonvanishing $\mu_{kf}$ (10). Quantitatively the rate of photo-induced ET from metal to molecule, as well as back ET from molecule to the metal substrate, can be taken as proportional to the square amplitude of the oscillating tail of the mixed wavefunction $|\mathrm{k}\rangle$ inside the metal. This tail is a schematic representation of the electronic coupling matrix element between the molecular resonance and the metal substrate. Note that Equation 1 applies to a one-color experiment under the CW approximation. In a pump-probe experiment with variable time delay, one needs to include the rate of decay from the transient molecular anionic resonance in the set of rate equations.

In Figure 1*b* the electronic interaction between the molecule and the metal substrate is weak. The coherent two-photon mechanism is not important here owing to the negligible matrix element for the excitation step. Instead, formation of the transient molecular anion is a result of scattering of the excited substrate electron into the molecular orbital. In the figure the wavefunction for the hot electron may represent different k values, not limited to $k_{||} = 0$. The tunneling barrier is determined by the nature of molecular spacers between the electron acceptor and the metal substrate. Such an indirect process can be distinguished from the direct mechanism in Figure 1*a* by the dependence of 2PPE yield on light polarization (9). The weak electronic coupling in Figure 1*b* should lead to a relatively long lifetime, and the electronic coupling matrix element should have a predominantly

tunneling contribution. The overall rate of this process is given by

$$w_{if} \propto w_{ik} \cdot \left|(\vec{\mu}_{kk} \cdot \vec{E})\right|^2, \qquad 2.$$

where $w_{ik}$ is the metal-to-molecule hot-electron tunneling rate, which has been treated in other contexts, such as hot-electron-induced resonant desorption, inelastic resonant electron-molecule scattering, and resonant tunneling. Interested readers are referred to this literature for details [(11) and references therein]. Pump-probe experiments are also applicable to this mechanism to establish the rate of ET.

In addition to the two major mechanisms illustrated in Figure 1, a transient molecular anion may also form indirectly from the decay of higher-lying electronic states, e.g., image states. However, the limited number of examples to date points to the dominance of the direct photo-excitation channel in 2PPE.

The two scenarios in Figure 1 illustrate the richness and power of the 2PPE technique in probing interfacial electronic structure and electron transfer dynamics. 2PPE is a particularly useful addition to more traditional surface spectroscopic techniques. For example, ultraviolet photoemission spectroscopy is limited to occupied electronic states (12). Inverse photoemission probes unoccupied electronic states [(13) and references therein] but has technical shortcomings, including limited energy resolution and the requirement for high electron fluxes that can easily damage molecular layers. Electron stimulated desorption has been successfully used to probe anionic resonances in a large number of adsorbate/metal systems that give desorption products from electron attachment (14). Other techniques such as X-ray absorption fine structure and electron energy loss spectroscopy provide limited probing of unoccupied electronic states. Compared to these traditional techniques, 2PPE is the only one capable of time-resolved measurements, particularly with time resolution compatible with ultrafast electron dynamics at interfaces.

Two-photon photoemission has been applied to the study of electron dynamics on metal and semiconductor surfaces, at metal-metal, metal-insulator, and metal-dielectric interfaces (10, 15–19). Recently, in this series, Harris and coworkers provided an authoritative review on 2PPE studies of image potential states at metal-adsorbate interfaces (20). These authors demonstrated the success in treating the adsorbate film as a dielectric layer and in elucidating the effects of such a dielectric layer on the energetics and dynamics of image states, on quantum well structures, and on polaron formation. In another chapter in this volume Petek & Ogawa probe an antibonding surface state formed from the adsorption of Cs on Cu(111) and demonstrate the use of time-resolved 2PPE in following the dynamics of Cs desorption (21).

In this account I focus on 2PPE studies of transient anionic resonances at molecule-metal interfaces and demonstrate this approach in addressing the central problem of interfacial ET. The review starts with a summary on experimental techniques, followed by a brief introduction to the dielectric continuum model. I then present experimental evidence for an anionic molecular resonance in a model system: hexafluorobenzene/Cu(111). The relationship of 2PPE results to interfacial ET dynamics is discussed. The next section addresses the important

role of polarization and localization. Substrate mediated surface photochemistry is discussed within the context of localization. Finally I present some perspectives on the role of 2PPE studies in addressing key issues in molecular and organic electronics before concluding with some comments.

## EXPERIMENTAL TECHNIQUES IN TWO-PHOTON PHOTOEMISSION



A 2PPE experiment can be carried out to determine the energetics, parallel dispersion, and lifetimes of interfacial electronic states. These experiments use laser light (one color or two color for pump-probe) with photon energies below the surface work function to avoid one-photon photoemission. Energetics are obtained in the spectroscopic mode, i.e., the kinetic energy of photo-emitted electrons are analyzed. The origins of photo-electrons from occupied, unoccupied, and final states can be easily distinguished based on the dependence of electron kinetic energy on photon energy. This is illustrated schematically for a one-color experiment in Figure 2, which shows three possible scenarios in 2PPE. In Figure 2*A* the absorption

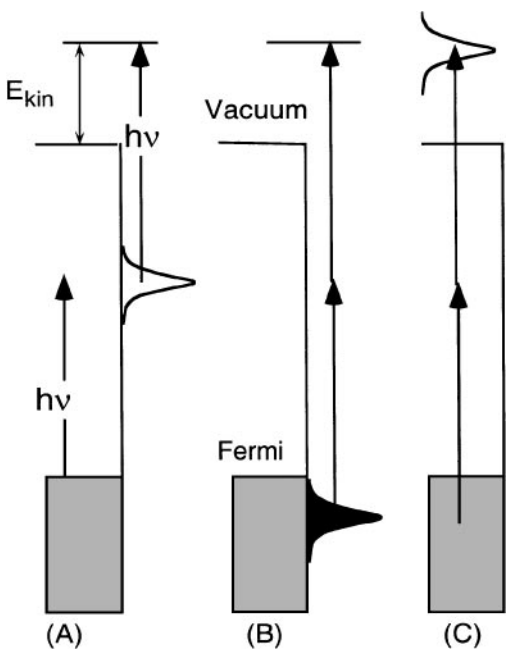


**Figure 2** Schematic illustration of three possibilities in two-photon photoemission involving unoccupied states below (*A*) or above (*C*) the vacuum level and an occupied state below the Fermi level (*B*).

of the first photon resonantly excites an electron from occupied metal bands to an unoccupied intermediate state; the absorption of a second photon excites this transient electron above the vacuum level. In this case the change in electron kinetic energy scales with that in photon energy, i.e., $\Delta E_{kin} = 1 \cdot \Delta h\nu$. In Figure 2*B* two-photon excitation from an occupied state leads to the ejection of an electron and $\Delta E_{kin} = 2 \cdot \Delta h\nu$. Finally, if the state is above the vacuum level, (Figure 2*C*) $E_{kin}$ is independent of photon energy. This can be viewed as a resonant scattering event in which the photo-excited electron resides transiently in the molecular orbital, followed by detachment and detection. Note the above simple arguments are only valid for interfacial states for which dispersion in the surface normal (z) direction is not important. They do not apply to bulk bands with dispersions in the z-direction.

Parallel dispersions of interfacial states are obtained in angle-resolved measurements. For an interface with long range order, the momentum parallel to the surface is conserved in the photoemission process. At an angle of detection of $\theta$ from the surface normal, the momentum parallel to the surface is obtained from the projection of the total linear momentum:

$$k_{//} = \sqrt{\frac{2m_e E_k}{\hbar^2}} \sin\theta, \qquad 3.$$

where $m_e$ is the electron mass, $E_k$ is the electron kinetic energy, and $k_{//}$ is the parallel momentum vector. The dispersion curve ($E_k$ vs. $k_{||}$) can be represented by an effective electron mass, $m_{eff}$, derived by fitting to the following free-electron–like parabolic function:

$$E_k = E_o + \frac{(\hbar k_{//})^2}{2m_{eff}}. \qquad 4.$$

The effective electron mass reflects the extent of localization/delocalization of the wavefunction in the surface plane.

Lifetimes of unoccupied electronic resonances (between the vacuum level and the Fermi level; Figure 2*A*) are derived from pump-probe measurements. In this case formation and ionization of the transient state are induced by two different laser pulses (often with different color) at a variable time delay. Lifetimes can be obtained from fitting the time-dependent signal with simple rate equations, provided the shape of the laser pulses in the time domain are well accounted for and calibrated. This kind of time-resolved measurement can be carried out with energy and angular resolution to provide a complete picture of the dynamics.

Early 2PPE experiments employed nanosecond dye lasers (for energetics and dispersion), but more recent experiments have used femtosecond lasers. Figure 3 shows a typical femtosecond 2PPE spectrometer available in my laboratory. It consists of a mode-locked Ti:sapphire oscillator pumped by an 8-W solid-state laser. The output from the oscillator (700–1000 nm, 76 MHz) is frequency doubled or tripled. The UV output can be split into two pulses for pump and probe.

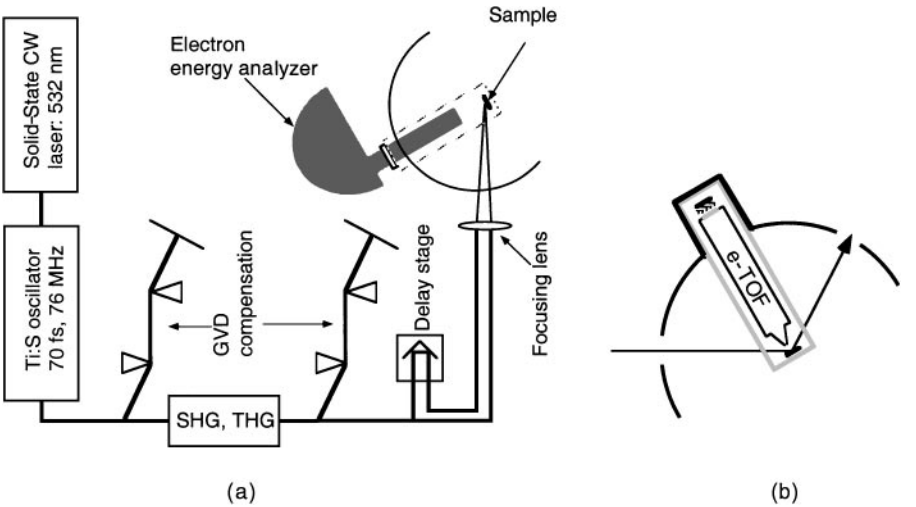


**Figure 3** (*a*) Schematics of femtosecond two-photon photoemission spectrometer with a hemispherical electron energy analyzer housed in an ultrahigh vacuum chamber. The laser system consists of a solid state pump laser and a tunable mode-locked Ti:sapphire oscillator. GVD, group velocity dispersion; SHG, second harmonic generation; THG, third harmonic generation. (*b*) Electron detection by a time-of-flight detector.

Alternatively the UV and residual fundamental can be used as pump and probe, respectively. Time delay between the two laser pulses is controlled by a translation stage. The pump and probe beams are focused slightly by an f = 50-cm lens and directed onto the surface of the sample located in an ultrahigh vacuum chamber. Photoelectrons are detected by a hemispherical analyzer. Variations of this setup include the use of an amplifier for better tunability, a time-of-flight detector for electron detection (20), and an interferometric setup for improved time resolution (18).

## IMAGE STATES AND THE DIELECTRIC CONTINUUM MODEL

To gain a better understanding of molecular anionic resonances, I first review a class of electronic states specific to interfaces: image states. This subject has been studied most extensively by 2PPE; interested readers are referred to several excellent review articles (15, 16, 20). The break of bulk symmetry at the crystalline surface gives rise to surface states that are confined to the interface in the surface normal direction but are of free electron Bloch wave character parallel to the surface. Among these, a series of unoccupied states at 1 eV or less below the vacuum level are the image states. Image states are of pure electrostatic origin. Consider an electron in front of and at a distance $z$ from a metal surface. The electron

induces polarization in the metal and the resulting positive charge cloud attracts the electron toward the surface. For a perfect metal the net result is equivalent to that of a Coulomb potential between the electron and a fictitious positive image charge (hence the name "image states") located at $-z$ inside the metal.

$$V_{im} = -\frac{e^2}{4\varepsilon z}, \qquad 5.$$

where $\varepsilon$ is the dielectric constant ($\varepsilon = 1$ for vacuum). If a project band gap exists in the surface normal direction, the electron is confined by the image potential on the vacuum side and the energy barrier on the metal side. A solution to this one-dimensional Hamiltonian gives a series of Rydberg states converging to the vacuum level. Note that image states are referenced to the vacuum level; the Fermi level does not come into the picture here. The consequence of this is made clear below.

What are the effects of an adsorbate layer on image states? The simplest picture involves treating the adsorbate layer as a dielectric film that screens the image potential ($\varepsilon > 1$). However, molecules are not mere dielectrics. They possess internal electronic structures and, in the case of an ordered film, energy bands. Consider the three scenarios in Figure 4.

In Figure 4*a* the adsorbate layer possesses negative electron affinity (EA). In other words, the bottom of the conduction band is above the vacuum level. The effective vacuum level or reference level ($V_{eff}$) an electron experiences when going from the vacuum side (*right*) through the molecular layer (*middle*) to the metal

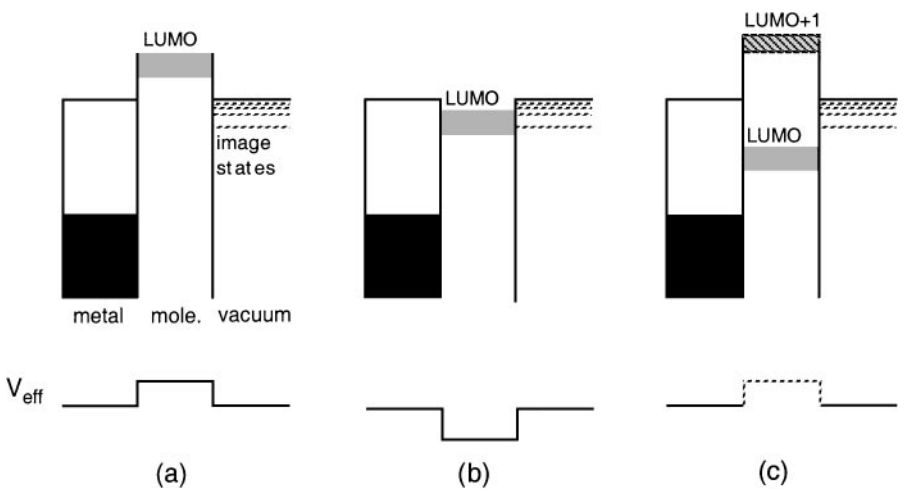


**Figure 4** Energy level diagrams showing the relative positions of the lowest unoccupied molecular orbital band with respect to the vacuum level in a metal-molecule-vacuum system. An effective vacuum level is shown below each energy level diagram. (*a*) Negative-electron affinity, (*b*) small positive-electron affinity, (*c*) large positive-electron affinity. Image states are shown as *dashed lines*.

side (*left*) is shown below the energy level diagram. The adsorbate layer serves as an effective energy barrier.

In Figure 4*b* the adsorbate layer is characterized by a small but positive EA, with the bottom of the conduction band (LUMO) below the image states. The effective potential is shown as having an attractive well within the adsorbate layer. However, this picture is only valid for image states located within the LUMO band. For image states above the top of the conduction band, the situation will be the same as in Figure 4*c*.

In Figure 4*c*, with a large, positive EA, the adsorbate LUMO band is below the image states. When an image-state electron tunnels through the adsorbate layer, the wavefunction contains a superposition of the LUMO band and some higher-lying bands, such as LUMO + 1. An accurate modeling of the effect of the adsorbate layer on image states requires a multiband coupling treatment. Intuitively, one expects the adsorbate layer to serve as a tunneling barrier.

When the effective potential picture does apply, the modified image states can be obtained from solutions to a Hamiltonian with potential equal to the sum of $V_{im}$ and $V_{eff}$ ($=-$EA) within the adsorbate layer:

$$V = -\frac{e^2}{4\varepsilon z} - EA \quad (0 < z < d), \qquad 6.$$

where $d$ is the thickness and $\varepsilon$ is the dielectric constant of the adsorbate layer. On the vacuum side (outside the adsorbate layer) the potential is given by the polarization of the composite interface:

$$V = -\frac{\beta e^2}{4(z-d)} + \frac{(1-\beta^2)\cdot e^2}{4\beta} \cdot \sum_{n=1}^{\infty} \frac{(-\beta)^n}{z-d+nd} \quad (z > d), \qquad 7.$$

where $\beta = (\varepsilon - 1)/(\varepsilon + 1)$. Inside the metal with a projected band gap, a two-band nearly free electron model is satisfactory.

The above is the dielectric continuum model (DCM) that Harris and coworkers (20) have applied successfully to a number of metal-dielectric interfaces with both positive and negative EA. As an illustration of the DCM, Figure 5 shows DCM simulation for the n = 1 image state on the naphthalene/Cu(111) surface (22). Owing to the attractive $V_{eff}$, the image state wavefunction becomes increasingly confined within the adsorbate layer with thickness. Note that for image states located within the adsorbate conduction band, a more accurate treatment requires the consideration of quantum well formation, i.e., image wavefunction confined by the thickness of the adsorbate layer. This requires treating the potential inside the adsorbate layer as a flat band, with an effective electron mass obtained from quantum well analysis, as has been done for Xe/Ag(111) (23).

A word of caution: The application of the DCM model to Figure 4*c*, in which the image states are located within the adsorbate band gap, is ill-considered. One may adjust parameters in the model to fit some aspects of experimental observation. The results are nevertheless unphysical.

Image states serve as excellent model systems for investigating the physics of electron dynamics at surfaces. They may couple strongly to molecular bands, as in

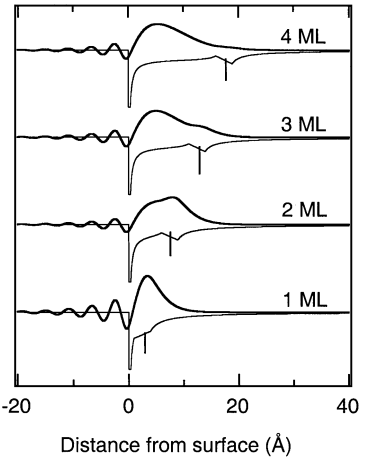


**Figure 5** Calculated image-state (n = 1) wavefunctions (*thick curves*) for 1–4 ML of naphthalene/Cu(111). The *thin dotted line* is the potential used. The position of z = 0 is the Cu(111)/adsorbate interface and the vertical line on each potential is the adsorbate/vacuum interface.



Figure 2*b*. However, of more interest to interfacial ET and molecular/organic electronics is probing molecular resonances directly. There have been a few examples in which transient anionic resonances have been observed in 2PPE spectra. These include the observation of the $\pi^*$ resonance in CO adsorbed on Cu(111) (24) and the $\sigma^*$ antibonding state in Cs adsorbed on Cu(111) and other metal surfaces [(25) and references therein]. Of a more controversial nature is the system of benzene on coinage metal surfaces. Whereas Wolf and coworkers reported the observation of the $\pi^*$ LUMO above the vacuum level (i.e., final state) for benzene adsorbed on Cu(111) (26), Harris and coworkers did not observe such a resonance on Ag(111) (27). An earlier claim of seeing the LUMO with vibrational fine structure for benzene/Cu(111) was not reproduced (28). Vondrak & Zhu first reported more definitive evidence for a transient anionic resonance for the system of hexafluorobenzene ($C_6F_6$) on Cu(111) (29–32). Below, I focus on this model system and discuss a few key issues in interfacial ET.

## MOLECULAR RESONANCES AND INTERFACIAL ELECTRON TRANSFER: A CASE STUDY OF $C_6F_6$/Cu(111)

The $C_6F_6$/Cu(111) system falls into the category of Figure 2*c*, in which the LUMO of the adsorbate layer is below the image states. Figure 6 compares 2PPE spectra for clean Cu(111), 1 ML $C_6F_6$/Cu(111), and 2 ML $C_6F_6$/Cu(111). The clean surface spectrum shows peaks owing to the d-band ($\sim$2 eV below $E_{Fermi}$), the occupied

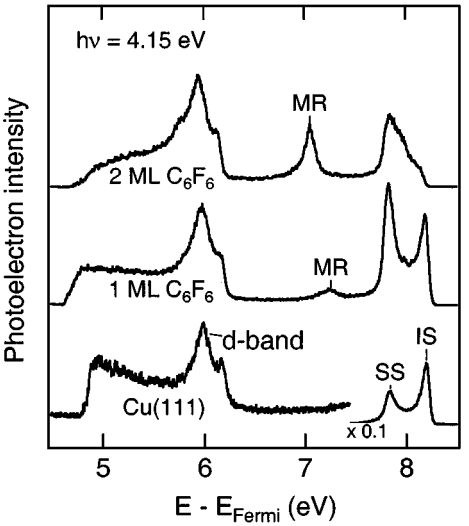


**Figure 6** Two-photon photoemission spectra for (bottom to top) Cu(111), 1 ML $C_6F_6$/Cu(111), and 2 ML $C_6F_6$/Cu(111). $h\nu = 4.15$ eV (29, 32).

surface state (0.4 eV below $E_{Fermi}$), and the unoccupied image state (n = 1, 0.84 eV below $E_{vac}$). The strong intensity of the surface and image state result in part from the fact that they are located within the projected bandgap from −0.85 eV (below $E_{Fermi}$) to 4.2 eV (above $E_{Fermi}$) for Cu in the ⟨111⟩ direction. After the adsorption of 1 and 2 ML of $C_6F_6$ both the surface state and the image state are attenuated and a new peak (labeled MR for molecular resonance) develops. The unoccupied nature of this resonance is established by the one-photon dependence of electron kinetic energy (Figure 7). This state is located at 3.18 and 2.99 eV above the Fermi level at 1 or 2 ML coverages, respectively. The coverage dependence in the position of the resonance is discussed below (see Figure 10). The observed resonance (MR) is assigned to the LUMO of $C_6F_6$ because it is well separated from the image states and because it is energetically located at a position expected from gas phase EA (29, 32). The vertical EA of gas phase $C_6F_6$ is ∼0 eV (adiabatic EA = 0.8 eV). The anionic resonance is stabilized by 0.8 eV in the condensed phase owing to polarization. Further stabilization of up to 1 eV is expected upon adsorption on the metal surface, owing to the image potential as well as wavefunction mixing between the LUMO and metal bands.

## Excitation Mechanisms

In principle a transient molecular anionic resonance can be formed from direct photo-excitation, hot-electron transfer, and indirect channels owing to the relaxation of higher-lying electronic states, such as image states. The limited number of examples to date have shown the dominance of the direct photo-excitation channel.

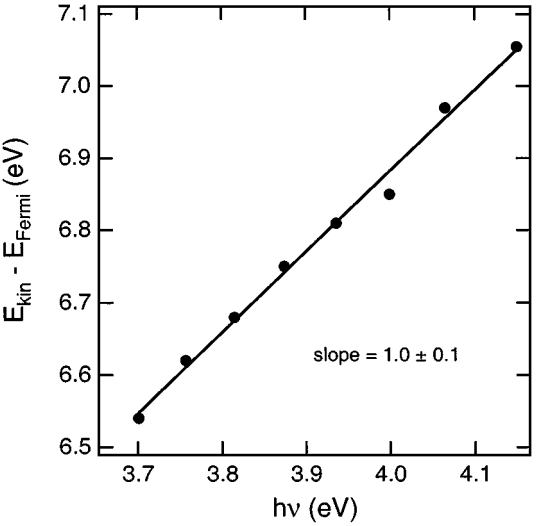


**Figure 7** Photo-electron kinetic energy for the molecular resonance as a function of photon energy for bilayer $C_6F_6$ on Cu(111) (29, 32).



Measurements of photoemission yields as a function of light polarization have established that populations of the $\sigma^*$ LUMO of $C_6F_6$ (33) and the $\pi^*$ LUMO in CO on Cu(111) (9) are both due to direct photo-excitation. The same is true for the Cs/Cu(111) system in which a resonance enhancement was observed for the surface state to $\sigma^*$ antibonding state excitation [(25) and references therein]. The direct photo-excitation mechanism is similar to the metal-to-ligand electron transfer mechanism in organometallic photochemistry.

The rate of photoemission in such a direct photo-excitation mechanism, given by Equation 1, is proportional to the square amplitude of the transition dipole moment, $\mu_{ik}$, for metal-to-molecule ET. A weakening in electronic coupling between the molecule and the metal should result in a decrease in $\mu_{ik}$ and, thus, a decrease in photoemission yield. This effect is observed experimentally in a recent 2PPE study of $C_6F_6$ on hydrogen-passivated Cu(111) (Figure 8) (32). With increasing coverage ($\theta$ = 0–0.34 ML) of preadsorbed atomic H, which systematically weakens the bonding between $C_6F_6$ and Cu(111), the 2PPE yield from the molecular resonance decreases by more than one order of magnitude. This is accompanied by an upward shift in energetic position by as much as 0.2 eV when $\theta_H$ increases from 0 to 0.34 ML. As the electronic interaction weakens, we expect the effect of stabilization of the transient anionic resonance by molecule-metal wavefunction mixing to diminish.

The requirement of nonvanishing $\mu_{ik}$ in the direct photo-excitation mechanism puts restrictions on the symmetry of the LUMO. Whereas the LUMO is readily observed in $C_6F_6$, it is invisible in pentafluorobenzene ($C_6F_5H$) on Cu(111) (31). For

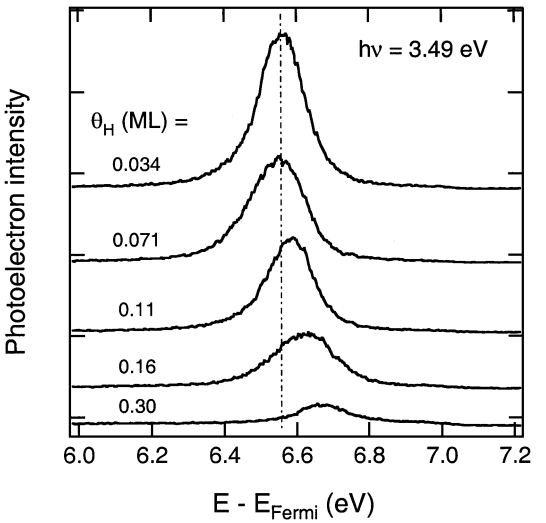


**Figure 8** Two-photon photoemission spectra of bilayer $C_6F_6$ on H/Cu(111) at the indicated surface hydrogen coverages (0.034–0.30 ML). Only the energy region for the molecular resonance is shown (32).



naphthalene and anthracene on Cu(111) (22, 34) and Ag(111) (35), the expected LUMOs based on gas phase EA were not seen in 2PPE, but they were readily observed in inverse photoemission [(13) and references therein]. The absence of a molecular resonance in 2PPE spectra may be attributed to vanishing $\mu_{\rm ik}$ owing to symmetry. This issue deserves further investigation.

In the case of Cs/Cu(111) direct photo-excitation into the $\sigma^*$ antibonding state was observed at very low coverages [(25) and references therein]. In this case the requirement of nonvanishing $\mu_{ik}$ may be satisfied by the fact the $\sigma^*$ state results from a combination of localized Cs atomic orbital and delocalized surface wavefunctions.

It is interesting to note that the hot-electron transfer mechanism (Figure 1*b*) has not been observed in the limited number of existing 2PPE studies. This mechanism must exist, as suggested by extensive evidence from surface photochemistry (5). I believe the direct observation of a transient anionic resonance from hot-electron transfer is only a matter of time, as more chemical systems are investigated by 2PPE. The same may be true for other indirect channels for transient anion formation. In this regard Ishioka et al. attributed the unusually short lifetime of image states on $C_6F_6$/Cu(111) to their efficient decay into the $\sigma^*$ LUMO (36).

## Intermolecular Interaction and Band Formation

Intermolecular interaction in molecular crystals results in the formation of electronic bands (37). This effect is more significant for unoccupied orbitals, such as LUMO and LUMO + n, than for occupied orbitals, owing to the fact that electronic

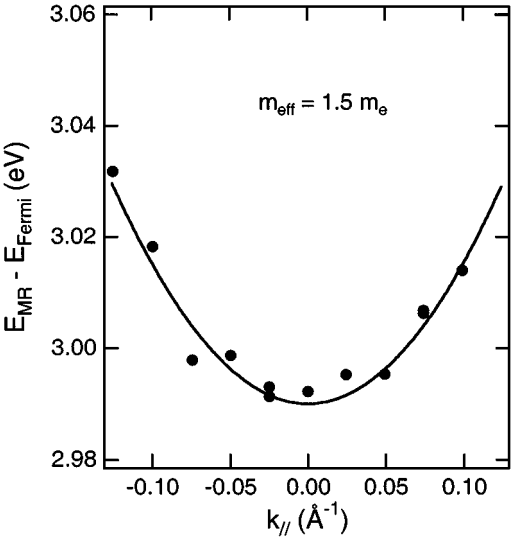


**Figure 9** Parallel dispersion curve for bilayer $C_6F_6$/Cu(111). The solid line is a fit to the free-electron–like equation that yields the indicated effective electron mass (32).



wavefunctions are more spatially diffuse at higher energies. The widths of conduction bands in van der Waals crystals are typically of the order of 0.1–0.2 eV (37) and, in some cases, can be as high as 0.5–0.6 eV (38). When adsorbed in an ordered structure on metal surface, the molecular anionic resonance can disperse into a conduction band owing to intermolecular electronic interaction and/or mixing with highly dispersed metal bands. In the direct photo-excitation mechanism discussed above, the presence of dispersion is required for nonvanishing $\mu_{ik}$.

The molecular anionic resonance in $C_6F_6$/Cu(111) displays significant dispersion. Figure 9 shows parallel dispersion of the molecular resonance for bilayer $C_6F_6$/Cu(111) obtained from angle-resolved 2PPE. The data can be fit to the free-electron-like parabolic dispersion in Equation 4 with an effective electron mass of 1.5 $m_e$. Experimental evidence points to the dominance of intermolecular interaction, not molecule-metal wavefunction mixing, as the source of such a highly dispersed molecular conduction band. Measurements of the dispersion of the molecular resonance in bilayer $C_6F_6$ on H/Cu(111) showed that $m_{eff}$ decreased from 1.5 $m_e$ on clean Cu(111) to 0.6 $m_e$ on 0.34 ML H covered surface. With the weakening of the molecule-surface interaction by preadsorbed H, intermolecular interaction energy plays a more important role in determining the overlayer structure. As a result, intermolecular packing is improved. This may explain the decrease in effective electron mass within the $C_6F_6$ LUMO band as the coverage of preadsorbed H increases. Gahl et al. showed that the effective electron mass decreases with increasing adsorbate layer thickness from 1.9 $m_e$ at 1 ML to 1.0 $m_e$ at 5 ML coverage (31). With increasing coverage, the role of the surface in

weakening intermolecular interaction is relaxed. As a result, we expect improved packing within the molecular layer to give better wavefunction overlap.

In view of the parallel dispersion and band formation, we expect that the molecular resonance should also disperse in the surface normal ($z$) direction for a film with finite thickness. Supporting this, one finds that the energetic position of the molecular resonance decreases with increasing thickness of the adsorbate film. A plausible interpretation of this observation is that the anionic resonance is stabilized owing to further delocalization (in the $z$ direction) as film thickness increases, or in other words, vertical dispersion. Such a vertical dispersion may be analyzed using quantum well or particle in a one-dimensional box analysis, as for Xe/Ag(111) (23). In the direction perpendicular to the quantum well, the delocalized LUMO wavefunction extends over but is also confined by the total thickness of the film. The boundary condition dictates that the quantum well wavefunction should contain a component of $\sin(k_z z)$, where the perpendicular wave vector is given by

$$k_z = \frac{n\pi}{d}, \qquad 8.$$

where $n$ (1, 2, . . .) is the quantum number of the quantum well state, $d$ ($Nd_o$) is the thickness of the molecular film, $N$ is the total number of molecular layers, and $d_o$ is the interlayer spacing. Taking $n = 1$ and using an average interlayer spacing of 5 Å for the solid $C_6F_6$ film (39), one can present the coverage dependence (31) of the molecular resonance position in the form of a perpendicular dispersion curve (Figure 10). The dashed curve is a fit of low $k_z$ data points to a free-electron-like

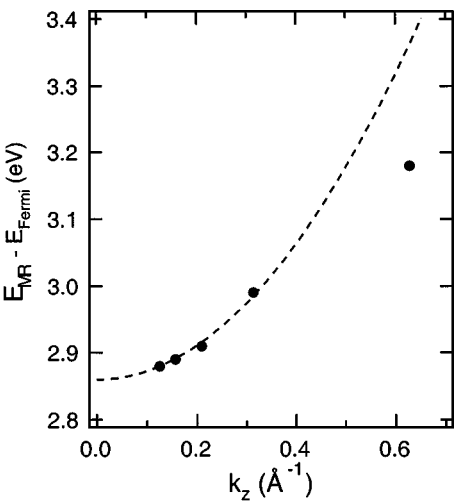


**Figure 10** Perpendicular dispersion for 1–5 ML $C_6F_6$/Cu(111) within the quantum well approximation. The *dashed line* is a fit to the free-electron–like equation for low $k_z$.

parabolic relationship:

$$E_k = E_o + \frac{(\hbar k_z)^2}{2m_{eff}}. \quad 9.$$

The fit yields an effective electron mass of 3 $m_e$ in the surface normal direction and puts the bottom of the molecular band at 2.86 eV. Note that such a quantum well picture predicts states at higher quantum numbers ($n > 1$). For 1(2) ML coverage, the $n = 2$ state is located at ~2 (0.5) eV higher than the $n = 1$ state and is not supported by the limited width of the molecular conduction band. However, for $C_6F_6$ coverages ≥3 ML, a weak and broad molecular resonance at ≤0.5 eV higher than the LUMO was indeed observed. Whether this broad peak is due to states at $n \geq 2$ remains an open question.



## Lifetimes and Molecule-to-Metal Electron Transfer

A transient anionic resonance, once formed, is subject to a number of dynamic processes, including polarization, localization, and decay to substrate states. The last is perhaps most important on a metal surface. Excited electronic states on metal surfaces are characterized by ultrashort lifetimes. This is due to the ease with which an electron in an excited molecular orbital can elastically transfer to the vast number of resonant electronic states (band) in the metal or can inelastically scatter with the large population of cold electrons at the Fermi sea. In the case of elastic molecule-to-metal ET, the lifetime, $\tau_{decay}$, of an excited molecular anion can often be correlated with the electronic coupling matrix element between the molecular orbital and the metal band structure: $1/\tau_{decay}$ is proportional to the square amplitude of the oscillating tail of the mixed wavefunction inside the metal (see Figure 1*a*). Thus, lifetime measurement provides a quantitative measure of the electronic coupling strength. Experimentally, this is done by varying the pump-probe delay time, with the pump laser pulse populating the anionic molecular resonance and the probe pulse ionizing the transient ion.

Figure 11*a* shows such a pump-probe experiment for 1–5 ML of $C_6F_6$ on Cu(111). Fitting to experimental data yields $\tau_{decay}$ shown in Figure 11*b*. The decay time increases from ~7 fs at 1 ML to ~32 fs at 5 ML coverage. The coverage dependence of the lifetime suggests that the electronic coupling between the LUMO and the metal surface weakens as film thickness increases. This is expected from dispersion in the surface normal direction. With increasing film thickness, the delocalized wavefunction (in the *z* direction) within the adsorbate layer is characterized by an increasing distance of the center-of-gravity of the wavefunction from the surface and a diminishing amplitude of the tail inside the metal.

Although thermal desorption measurement indicates that $C_6F_6$ is weakly adsorbed on the Cu(111) surface (29), the lifetime of ~7 fs for the LUMO at monolayer coverage is of the same order as those in strong chemisorption systems determined by both experiment and theory. For example, the lifetime of the $\pi^*$ anionic resonance in CO chemisorbed on Cu(111) was measured to be $1 < \tau < 5$ fs

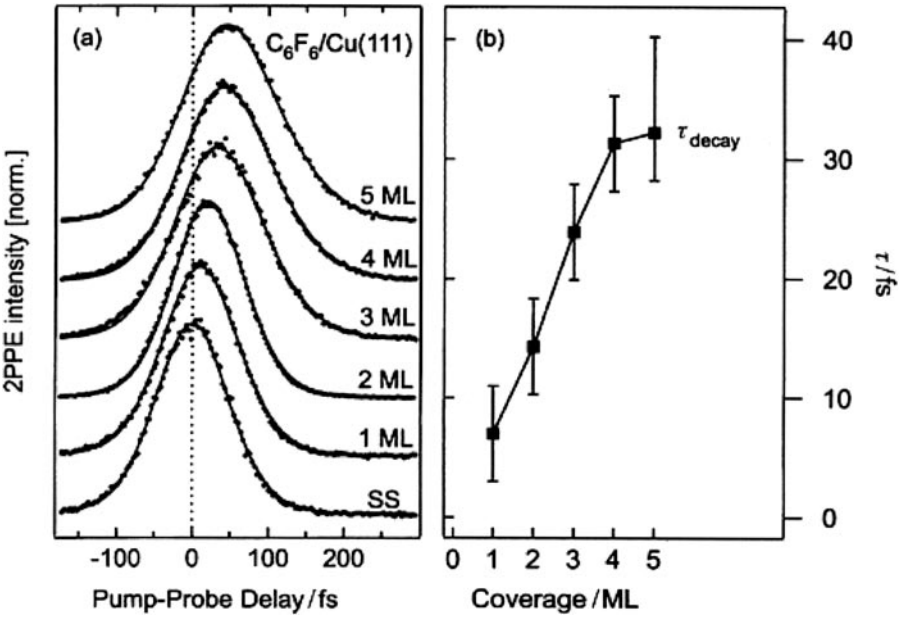


**Figure 11** Time-resolved two-photon photoemission spectroscopy. (*a*) Cross-correlation curves of the molecular resonance of $C_6F_6$/Cu(111) at the indicated coverages, recorded with $h\nu_1 = 4.26$ eV pump and $h\nu_2 = 2.13$ eV probe pulses. The *dotted line* indicates zero delay time determined from the cross-correlation signal of the occupied surface state (SS) on clean Cu(111). (*b*) Lifetimes (population decay) for the molecular resonance as a function of coverage. Note that a finite rise time was included to obtain a satisfactory fit. After Gahl et al. (31).

by time-resolved 2PPE and spectral line width (40), whereas those for the $\sigma^*$ antibonding states in alkali atoms on metal surfaces range from a few femtoseconds to a few tens of femtoseconds [(25) and references therein]. The electronic coupling strength between an unoccupied molecular orbital and the metal substrate is not immediately obvious from bonding strength because LUMOs are often not involved to a great extent in bonding.

Whereas the measured lifetime for the $\sigma^*$ anionic resonance in $C_6F_6$/Cu(111) indicates efficient molecule-to-metal resonant (elastic) electron transfer and/or inelastic electron scattering, the actual ET mechanism is not clear. The $\sigma^*$ LUMO of $C_6F_6$ is located within the projected bandgap of Cu(111). Elastic ET from $\sigma^*$ LUMO of $C_6F_6$ to resonant metal states at or near $k_{||} = 0$ is forbidden. In such a band picture the barrier for elastic ET increases as $k_{||}$ increases [(25) and references therein]. However, as discussed in more detail below, polarization effects (electronic, intramolecular, and intermolecular) can relax the momentum requirement in resonant ET. A localized state essentially possesses all *k* components, and

the band picture becomes invalid. As a result, elastic ET becomes allowed. On the other hand, decay of the $\sigma^*$ resonance owing to inelastic scattering with the vast number of Fermi electrons is not restricted by the presence of a projected bandgap. The relative importance of each channel is not known; this is an excellent problem for further experimental and theoretical studies.

## POLARIZATION AND LOCALIZATION

Molecule-to-metal electron transfer is not the only process for the molecular resonance. Once formed, the transient molecular resonance is subject to a number of dynamic processes, such as electronic polarization, nuclear polarization, localization, chemical changes, and other inelastic scattering events. These dynamic processes must be considered because we are employing concepts of single-electron excitation in describing an inherently multibody problem. I now present a qualitative analysis of this complex picture. Interested readers may find relevant concepts in the fascinating book on organic molecular crystals by Silinsh & Capek (37) and in several excellent review articles on surface electron dynamics (17, 18, 20).

### Competition Between Delocalization and Localization

The complex dynamics following the excitation of a molecular anionic resonance on a metal surface is illustrated schematically in Figure 12 based on two axes: the spatial localization of excitation and the relaxation of excitation energy. This process is a result of competition between delocalization and localization, the conditions for which can be intuitively understood from energetic considerations based on two inequalities introduced below.

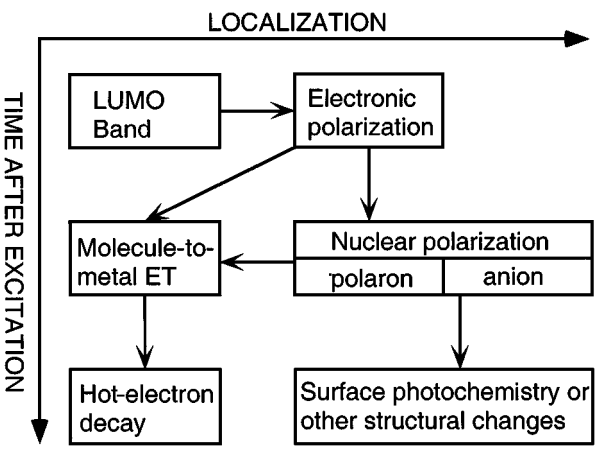


**Figure 12** Schematic illustration of dynamic processes for a transient molecular resonance.

For an excited molecular anionic resonance, delocalization is determined by the resonant interactions between neighboring molecular orbitals and between a molecular orbital and metal band structure. Both processes are characterized by electronic coupling matrix elements or transfer integrals (37): $J_{MM}$ and $J_{MS}$ for intermolecular and molecule-substrate electron transfer, respectively. The values of these transfer integrals are of the same order as bandwidths. For molecular crystals, $J_{MM}$ is of the order of a few tenths of eV. For molecule-metal interactions, $J_{MS}$ for an excited molecular orbital can be as high as 1 eV [(41) and references therein]. For large values of $J_{MM}$, the wavefunction in the molecular layer is a Bloch wave with definitive wave vector, $\boldsymbol{k}$. This picture, similar to that in inorganic semiconductors, is valid when the mean-free-path of the excited electron is significantly larger than the lattice parameter or intermolecular distance. For large values of $J_{MS}$, the molecular wavefunction is strongly mixed with Bloch-type waves of the metal substrate. A consequence of large values of $J_{MS}$ is the ultrafast rates of ET between the metal and the molecule. In the limit of strong coupling, the rate approaches the Bohr frequency, and ET is essentially a charge redistribution process within the mixed wavefunction. The two delocalization effects result in energy gains (stabilization) represented by $\delta E_{del\text{-}MM}$ and $\delta E_{del\text{-}MS}$ for intermolecular and molecular-substrate delocalization, respectively. Both are negative values of the order of transfer integrals.

The opposite trend is localization, which is determined by polarization in electronic and nuclear coordinates of the surrounding environment. An excess electron in an adsorbate film induces charge redistribution in the valence wavefunctions of neighboring molecules as well as in the metal substrate. Such an electronic polarization process occurs on the timescale of the inverse of the Bohr frequency, i.e., $10^{-16}$–$10^{-15}$ s. One may also estimate this timescale from the electronic excitation energy based on the uncertainty principle. Because this timescale is substantially shorter than that for the movement (hopping) of a localized electron from one molecule to another, we can simply consider the electronic polarization effect as the total electrostatic attraction between a fixed electron and induced dipoles in surrounding neutral molecules and in the metal substrate; the latter is the image potential discussed earlier. These electrostatic attraction potentials create a localized trap for the electron. Additional localization comes from polarization of nuclear subsystems on a longer timescale. There are two main flavors: intramolecular polarization, i.e., vibronic coupling and molecular polaron formation ($10^{-14}$ s), and intermolecular polarization, i.e., lattice polaron formation ($\sim 10^{-13}$ s). The timescale in each case is the inverse of the frequency involved, intramolecular vibrations or lattice phonons. I discuss polarization and localization of the nuclear subsystem in more detail below.

Both electronic and nuclear polarizations lead to energy gain, $\delta E_{loc}$, for the localization of the electron. The magnitude of $|\delta E_{loc}|$ is of the order of eV, depending on the polarizability of molecules and dipole moments for vibrational excitation. In addition to polarization energy, the localized electron can also form direct bonding with a molecule, resulting in an anion. In other words, the electron resides in

a particular molecular orbital. This is accompanied by an energy gain of $\delta E_b$.

If the following inequality is satisfied,

$$|\delta E_{del-MM} + \delta E_{del-MS}| > |\delta E_{loc} + \delta E_B|, \quad 10.$$

the delocalization trend wins, and the dynamic process is dominated by the left side of Figure 12. Excitation is quenched owing to hot-electron decay on a $10^{-15}$–$10^{-14}$ timescale. This is the fate for molecular layers with relatively broad bandwidth and/or with strong molecule-metal electronic coupling.

If the opposite is true, i.e.,

$$|\delta E_{del-MM} + \delta E_{del-MS}| < |\delta E_{loc} + \delta E_B|, \quad 11.$$

localization dominates, and this leads to the right side of the dynamic pathway in Figure 12: the excitation of molecular and lattice vibrations, as well as chemical or structural changes. This applies to narrow bandwidth molecular films and weak molecule-metal coupling; instead of a Bloch-type wave, the wavefunction is better described by a localized quasi-particle.

There are two important issues one must remember in applying the inequalities. First, these inequalities should only serve as qualitative guidelines, not quantitative criteria dictating dynamics. Time is of the essence. For example, energetic conditions favoring localization, such as polaron formation and surface photochemistry, may not be observed experimentally because the timescale for localization could be too slow to compete with delocalization with the metal (resonant molecule-to-metal ET). On the other hand, inelastic scattering events may also lead to localization under conditions favoring delocalization. Second, the picture in Figure 12 starts with direct photo-excitation of a resonance with nonvanishing dispersion. However, inelastic scattering may lead to the formation of a localized molecular anion directly from hot electron transfer (Figure 1*b*), thus bypassing the dynamic steps leading to localization. In this scenario the dynamic process is a competition among the following possibilities: resonant molecule-to-metal ET, inelastic scattering with metal electrons at the Fermi sea, and chemical/structural changes.

The case study of $C_6F_6$/Cu(111) may fall into the category of Equation 10. Angle-resolved measurement showed no sign of localization; there were no features of nondispersive states within the lifetime of the molecular resonance. A minor photo-dissociation channel may be attributed to the direct formation of localized anions from hot-electron transfer/scattering events (31, 32). Whereas the molecular resonance was observed in 2PPE spectra at photon energies above the energetic threshold, the photo-dissociation channel was only observed at high photon energies; this can be attributed to the low cross sections for hot-electron transfer or inelastic scattering at low photon energies (e.g., $h\nu = 3.49$ eV) (Figure 8).

The only example of polaron formation at adsorbate/metal interfaces came from the work of Harris and coworkers (42). These authors showed that image-state electrons in the alkane/Ag(111) system can be trapped at the surface of the alkane film, leading to the formation of small polarons (mainly two-dimensional). The decay dynamics of delocalized image states to localized small polarons was directly

followed in time- and angle-resolved 2PPE. Similar experiments for molecular resonances are warranted in the near future.

## Molecular Polarons and Surface Photochemistry

Charge localization due to polarization of nuclear subsystems is of particular interest not only because it is an integral part of the dynamic process but also because it can lead to chemical and structural consequences. The following nuclear coordinates need to be considered: intramolecular and molecule-surface vibrations. The timescale ($\Delta t$) for each interaction can be estimated from the characteristic vibrational frequency based on the uncertainty principle: $\Delta E \Delta t = h\nu\Delta t \approx h$; thus, $\Delta t \approx 1/\nu$.

Polarization of intramolecular coordinates results in a molecular polaron or a transient anion. If dipole active vibrational modes in neighboring molecules are also involved in trapping the molecular polaron, the net result is a nearly small molecular polaron. Typical intramolecular vibrational frequencies of 3000–300 $cm^{-1}$ correspond to interaction times of $2 \times 10^{-15}$–$2 \times 10^{-14}$ s. For the molecule-surface coordinate, the interaction time is of the order of $10^{-14}$ s. These timescales compete with that for molecule-to-metal ET on a similar or shorter timescale. Polaron hopping (to neighboring molecules) occurs on a longer timescale and is not competitive. During the lifetime of the molecular polaron, i.e., the residence time of the electron on the molecule, the molecule evolves from the equilibrium configuration for the neutral to that for the negatively charged state. Thus, following the decay of the molecular polaron, intramolecular and molecule-surface vibrations are excited. Whereas vibrational excitations within the adsorbate layer may be eventually dissipated to the phonon bath of the substrate metal, a competitive channel is that of chemical change, i.e., surface photochemistry. In fact, the above description for polaron formation and decay is identical to the widely accepted model of hot electron–mediated surface photochemistry, within the frameworks of the Menzel-Gomer-Redhead (MGR) and Antoniewicz models for photodissociation and desorption (5).

In an account entitled "Surface Photochemistry" in this series eight years ago, I concluded that the majority of photochemical processes on metal surfaces could be attributed to hot-electron mechanisms (5). Thus, metal surface photochemistry is part of the big picture for polarization and localization of an excited electron; in other words, surface photochemistry results from the decay of molecular polarons. However, most experimental evidence has shown that the rate of hot electron–mediated surface photochemistry scales with light absorbance in the metal, not with electric field strength (5). One must then conclude that the direct photoexcitation mechanism (Figure 1*a*) is not responsible in these systems. Rather, localized molecular polarons or anions form directly from the hot-electron scattering or tunneling mechanism in Figure 1*b*. In most surface photochemical systems investigated to date, molecular anionic resonances should be of highly localized character. The small intermolecular transfer integral, $J_{MM}$, points to the invalidity of the electronic band picture and excludes the direct photo-excitation mechanism.

In fact, the localized nature of these anionic resonances is the reason for the competitiveness of photochemical pathways. One can also predict that adsorbate systems featuring large $J_{MM}$ values and, hence, delocalized electronic bands, are unlikely candidates for surface photochemistry.

In another chapter in this volume Petek & Ogawa (21) present an elegant 2PPE study of the photodesorption dynamics of Cs from Cu(111) at low adsorbate coverages. The $\sigma^*$ antibonding resonance is populated by direct photo-excitation. In this case the requirement for delocalization was satisfied by the large adsorbate-substrate transfer integral, $J_{MS}$, not the interadsorbate interaction, $J_{MM}$. Photodesorption dynamics is essentially localization dynamics. As the Cs-surface bond stretches, $J_{MS}$ decreases and the excited electron is increasingly localized to the adsorbate.



## IMPLICATIONS FOR MOLECULE ELECTRONIC DEVICES

The use of molecules in electronic devices is attractive for a number of reasons, among them, the great flexibility for tuning electronic properties by chemical modification and the natural scalability to the nanometer or single molecule level. One can divide molecule-based electronic devices into two categories: conventional devices using molecular semiconductors and molecular electronics using one or a small group of molecules. The issues of electronic structure and electron transfer dynamics addressed by 2PPE are of fundamental importance to the understanding and design of both types of devices. I use three examples below to illustrate my point.

### Energetics and Dynamics

Recent demonstration of high mobility field effect transistors (FETs) including superconducting FETs based on molecular crystals (43–46) such as pentacene, tetracene, and $C_{60}$ have attracted considerable interest in these molecular materials. In such devices, charge transport is often determined by a single or a few molecular layers at the interface. Thus, understanding the band structure of these molecular thin films is critical. 2PPE is perhaps the most powerful technique in establishing the structure of conduction bands. For example, Figure 13 shows a set of 2PPE spectra taken for bilayer $C_{60}$ epitaxially grown on Cu(111). The spectral dependence on $h\nu$ establishes three unoccupied states, LUMO, LUMO + 1, and LUMO + 2, and the highest occupied molecular orbital. Time-resolved experiments are necessary to characterize the dynamics of electrons in each unoccupied state and the dependence of dynamics on momentum and temperature. These dynamics measurements can establish quantitatively the electron-phonon coupling, which is responsible for the transition from band conduction at low temperatures to polaron-hopping conduction at high temperatures (47). For example, a recent 2PPE study determined, for the first time, the electron-phonon coupling constant in carbon nanotubes (48).

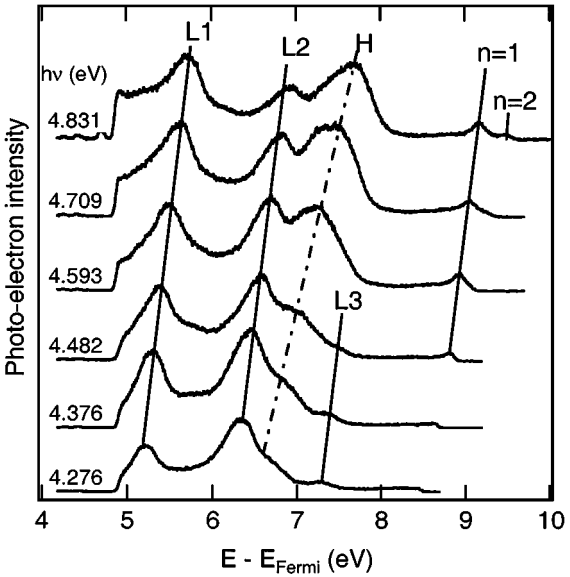


**Figure 13** Two-photon photoemission spectra of 2 ML C60/Cu(111) taken with one-color laser light at the indicated photon energies. The *solid lines* correspond to one-photon dependence and the *dot-dashed line* is a two-photon dependence in peak positions. H, HOMO; L1, LUMO; L2, LUMO+1; L3, LUMO+2; image states (n = 1, 2). (G. Dutton & X.-Y. Zhu, unpublished results).

## Delocalization or Localization?

In FETs based on molecular crystals the figure of merit is carrier mobility. Band formation owing to delocalization or a large transfer integral is most desirable. Localization and polaron formation can only decrease carrier mobility and should be minimized in molecular design and crystal engineering.

Is the same true for molecular electronics? The answer is probably "no." For a molecular device to function, one would like to see changes in electronic properties, such as conductivity, to occur locally. In this sense delocalization owing to large transfer integrals between molecules or between a molecule and a metal electrode is undesirable. Instead, the figure of merit should be the strong tendency to localize owing to electronic and nuclear polarization. Recently, negative differential resistance and switching effects have been observed in two-terminal devices based on single or a group of conjugating molecules assembled on metal electrodes (Figure 14) (4, 49). A possible interpretation is that when an electron passes through the molecule, the strong polarization effect from electron-vibration coupling may lead to the formation of a molecular polaron, which shuts off further electron transport. Even after the decay of the molecular polaron, the resulting excitation in nuclear coordinates may lead to meta-stable structural or conformational

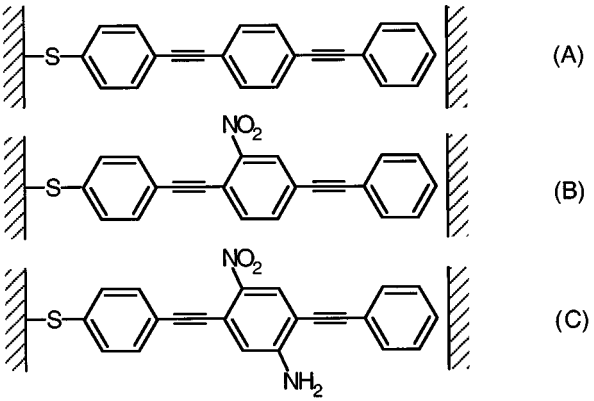


**Figure 14** Molecules for which negative differential resistance or switching effects were observed (4, 49).



change that gives rise to the switching behavior. The fact that negative differential resistance or switching in molecules in Figure 14*B*, *C* is much more significant than that in Figure 14*A* supports the argument of localization. The addition of the $-NO_2$ group to the middle phenyl ring not only enhances electron-vibration coupling owing to the increased vibrational dipole moment but also creates a more efficient trap for the molecular polaron.

## The Contact Problem

Making electronic contact to molecules is critical in both conventional and single-molecule devices. In organic FETs and light-emitting devices this is the charge injection issue. Energetics is not the only factor to consider in charge injection. Both electronic coupling and interfacial relaxation dynamics, as discussed extensively in this account, are important to charge injection at interfaces. These issues are not easy to probe in device measurements. Frisbie and coworkers recently carried out transport measurements using conduction-probe atomic-force microcopy to make nano-contacts to organic crystals or self-assembled monolayers (SAMs) (50, 51). These experiments clearly point to the critical importance of contacts. A recent experiment by Houston and coworkers established the role of contact pressure on conductance through alkanethiol SAMs (52).

The importance of contacts only increases as device dimensions decrease, particularly to the molecular level. For example, SAMs of thiols on metal surfaces have been popular choices in the construction and testing of molecular electronic devices. The easy formation of the thiolate-metal contact is an attractive method to connect molecular components to metal electrodes. The questions are: What is the electronic structure of the thiolate-metal contact? How does this contact affect electron transport through the molecular wire? Recent 2PPE measurements and ab

initio calculations on model SAM/Cu(111) systems (53) showed the presence of two $\sigma^*$ states localized to the C-S-Cu linker. For symmetry reasons these localized $\sigma^*$ states introduced by the anchoring bond cannot couple to the delocalized $\pi^*$ states within a conjugated molecular framework. Thus, the thiolate contact can be considered insulating for electron transport through a self-assembled monolayer of molecular wires. On the other hand, ab initio calculation showed that the highest occupied molecular orbital ($\pi$) is delocalized between the molecular framework and the metal surface via the –S-bridge. Therefore, unlike for electron transport, the thiolate contact is conducting for hole transport.



## COMMENTS

To recycle a sentence from eight years ago, I hope the key issues addressed in this account have raised more questions than provided answers (5). The application of 2PPE to interfacial electronic structure and electron transfer dynamics is only beginning to show its exceptional attractiveness. These studies allow us to probe the central issue of interfacial ET and to provide a unified view on many exciting research areas. In the current rush toward demonstrating molecular electronic devices, it may be helpful to pause for a moment and consider some of the physical chemistry principles we can learn from the kind of fundamental studies demonstrated here. Whereas experimental work using time- and angle-resolved 2PPE on more model systems is needed, theoretical work will also be essential to guarantee the success of this research field.

## ACKNOWLEDGMENTS

I thank my students and coworkers, particularly Gregory Dutton, for most of the experimental results included in this account and for a critical reading of the manuscript. This work was supported by the National Science Foundation (DMR-9982109) and the University of Minnesota. Acknowledgement is made to the donors of the Petroleum Research Fund, administrated by the American Chemical Society, for partial funding of this work.



## LITERATURE CITED

1. Salaneck WR, Brédas JL. 1997. *MRS Bull.* 22:46–51
2. Brutting W, Berleb S, Muckl AG. 2001. *Organ. Electron.* 2:1–36
3. Garnier F, Kouki F, Hajlaoui R, Horowitz G. 1997. *MRS Bull.* 22:52–56
4. Chen J, Reed MA, Rawlett AM, Tour JM. 2000. *Science* 286:1550–52
5. Zhu X-Y. 1994. *Annu. Rev. Phys. Chem.* 45: 113–44
6. Hagfeldt A, Gratzel M. 1995. *Chem. Rev.* 95:49–68

7. Miller RJD, McLendon GL, Nozik AJ, Schmickler W, Willig F. 1995. *Surface Electron Tansfer Processes*. New York: VCH
8. Bard AJ, Faulkner LR. 2001. *Electrochemical Methods: Fundamentals and Applications*. New York: Wiley. 2nd ed.
9. Wolf M, Hotzel A, Knoesel E, Velic D. 1999. *Phys. Rev. B* 59:5926–35
10. Hofer U, Shumay IL, Reuss Ch, Thomann U, Wallauer W, Fauster Th. 1997. *Science* 277:1480–82
11. Gadzuk JW. 1995. *Surf. Sci.* 342:345–58
12. Bonzel HP, Kleint C. 1995. *Prog. Surf. Sci.* 49:107–53
13. Frank KH, Yannoulis P, Dudde R, Koch EE. 1988. *J. Chem. Phys.* 89:7569–77
14. Sanche L. 2000. *Surf. Sci.* 451:82–90
15. Fauster Th, Steinmann W. 1995. In *Photonic Probes of Surfaces*, ed. P Halevi. Amsterdam: Elsevier
16. Osgood RM Jr, Wang X. 1998. *Solid State Phys.* 51:1–80
17. Haight R. 1995. *Surf. Sci. Rep.* 21:275–325
18. Petek H, Ogawa S. 1998. *Prog. Surf. Sci.* 56:239–311
19. Aeschlimann M, Bauer M, Pawlik S. 1996. *Chem. Phys.* 205:127–41
20. Harris CB, Ge N-H, Lingle RL Jr, McNeill JD, Wong CM. 1997. *Annu. Rev. Phys. Chem.* 48:711–44
21. Petek H, Ogawa S. 2002. *Annu. Rev. Phys. Chem.* 53:507–31
22. Wang H, Dutton G, Zhu XY. 2000. *J. Phys. Chem. B* 104:10332–38
23. McNeill JD, Lingle RL, Jordan RE, Padowitz DF, Harris CB. 1996. *J. Chem. Phys.* 105:3883–91
24. Hertel T, Knoesel E, Hasselbrink E, Wolf M, Ertl G. 1994. *Surf. Sci.* 317:L1147–51
25. Petek H, Nagano H, Weida MJ, Ogawa S. 2001. *J. Phys. Chem. B* 105:6767–79
26. Velic D, Hotzel A, Wolf M, Ertl G. 1998. *J. Chem. Phys.* 109:9155–65
27. Gaffney KJ, Wong CM, Liu SH, Miller AD, McNeill JD, Harris CB. 2000. *Chem. Phys.* 251:99–110
28. Munakata T, Sakashita T, Tsukakoshi M, Nakamura J. 1997. *Chem. Phys. Lett.* 271: 377–80
29. Vondrak T, Zhu X-Y. 1999. *J. Phys. Chem. B* 103:3449–56
30. Zhu X-Y, Vondrak T, Wang H, Gahl C, Ishioka K, Wolf M. 2000. *Surf. Sci.* 451: 244–49
31. Gahl C, Ishioka K, Zhong Q, Hotzel A, Wolf M. 2000. *Faraday Discuss.* 117:191–202
32. Dutton G, Zhu X-Y. 2001. *J. Phys. Chem. B* 105:10912–17
33. Gahl C. 1999. Diploma thesis. Fritz Haber Inst., Berlin
34. Wang H. 2001. PhD thesis. Univ. Minnesota, Minneapolis
35. Gaffney KJ, Liu SH, Miller AD, Szymanski P, Harris CB. 2000. *J. Chin. Chem. Soc.* 47:759–63
36. Ishioka K, Gahl C, Wolf M. 2000. *Surf. Sci.* 454:73–77
37. Silinsh EA, Capek V. 1994. *Organic Molecular Crystals: Interaction, Localization, and Transport Phenomena*. Woodbury, CT: AIP
38. Cornil J, Calbert JPh, Bredas JL. 2001. *J. Am. Chem. Soc.* 123:1250–51
39. Boden N, Davis PP, Stam CH, Wesselink GA. 1973. *Mol. Phys.* 25:81–88
40. Bartels L, Meyer G, Rieder KH, Velic D, Knoesel E, et al. 1998. *Phys. Rev. Lett.* 80: 2004–7
41. Braun J, Nordlander P. 2000. *Surf. Sci.* 448:L193–99
42. Ge NH, Wong CM, Linge RL Jr, McNeill JD, Gaffney KJ, Harris CB. 1998. *Science* 279:202–5
43. Schon JH, Kloc Ch, Batlogg B. 2000. *Nature* 406:702–4
44. Schon JH, Kloc Ch, Haddon RC, Batlogg B. 2000. *Science* 288:656–58
45. Schon JH, Kloc Ch, Batlogg B. 2000. *Science* 288:2338–40
46. Schon JH. 2001. *Synth. Metals* 122:157–60
47. Schon JH, Kloc Ch, Batlogg B. 2001. *Phys. Rev. Lett.* 86:3843–46

48. Hertel T, Moos G. 2000. *Phys. Rev. Lett.* 84:5002–5
49. Donhauser ZJ, Mantooth BA, Kelly KF, Bumm LA, Monnell JD, et al. 2001. *Science* 292:2303–7
50. Kelley TW, Granstrom EL, Frisbie CD. 1999. *Adv. Mater.* 11:261–64
51. Wold DJ, Frisbie CD. 2000. *J. Am. Chem. Soc.* 122:2970–71
52. Son KA, Kim HI, Houston JE. 2001. *Phys. Rev. Lett.* 86:5357–60
53. Vondrak T, Wang H, Winget P, Cramer CJ, Zhu X-Y. 2000. *J. Am. Chem. Soc.* 122: 4700–7

*Annual Review of Physical Chemistry*
*Volume 53, 2002*

# CONTENTS